

http://pubs.acs.org/journal/aesccq Article

Brown Carbon Formation Potential of the Biacetyl-Ammonium Sulfate Reaction System

Daisy N. Grace, Emily N. Lugos, Shiqing Ma, Daniel R. Griffith, Heidi P. Hendrickson, Joseph L. Woo, and Melissa M. Galloway*



Cite This: https://dx.doi.org/10.1021/acsearthspacechem.0c00096



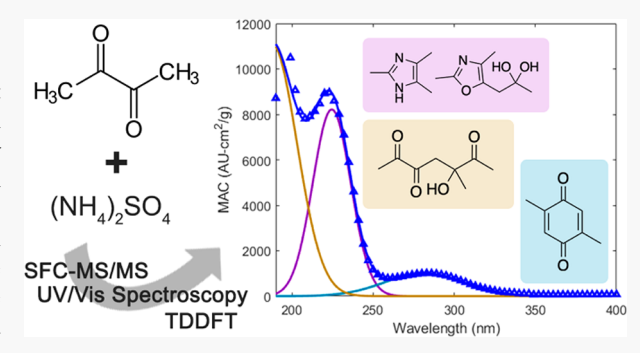
ACCESS

III Metrics & More

Article Recommendations

s Supporting Information

ABSTRACT: The contribution of organic aerosol from biomass burning is poorly constrained, and the lack of consensus regarding its overall contribution to global radiative forcing leads to significant uncertainties in climate modeling. Identification of potential brown carbon chromophores from common biomass burning emissions may reduce this uncertainty. Biacetyl (BA) is found in emissions from industry and biomass burning from various ecosystems and shares structural similarities with other small carbonyls that react with ammonium sulfate (AS) to produce brown carbon compounds. Like previous carbonyl + AS studies, the BA + AS system results in the formation of hundreds of different products; these were separated and identified using supercritical fluid chromatography—tandem mass



spectrometry, isotopic substitution experiments, and comparisons to standards. Kinetic information was obtained through spectral decomposition of experimentally measured UV—visible absorbance data. Theoretical TDDFT calculations were utilized to extract more information on the light absorbance of identified products and to determine how these individual chromophores would contribute to the light absorbance of organic aerosol. This information could provide insight into unknown organic aerosol behavior by furthering our understanding of the reactivity of a common biomass burning emission product like biacetyl.

KEYWORDS: biacetyl, brown carbon, imidazole, oxazole, quinone, pyrrole, furanone

■ INTRODUCTION

With projections for wildfire frequency on the rise in the U.S., understanding the extent of environmental health impacts associated with biomass burning (BB) has become critical in recent years. BB contributes significant concentrations of black carbon aerosol and organic aerosol (OA) emissions, both of which influence global positive radiative forcing. Black carbon radiative forcing effects are better understood in their consideration in global climate models and contribute more significantly than OA. The struggle to capture the complexities of the OA component in determining the global energy budget, however, has contributed to large uncertainties in these models for both black carbon and OA estimates. 1-3,5

The wide variety of structural differences in OA results in aerosol that can scatter and/or absorb sunlight, the latter of which is considered brown carbon (BrC). BB generates BrC both directly, where BrC aerosol are emitted as OA, and indirectly, where volatile gases emitted from BB undergo oxidative aging reactions that lead to secondary OA (SOA) that can undergo further aging and BrC evolution. ^{1–3,5,6} Because of the multifaceted nature of SOA formation, field and laboratory studies measuring BB SOA are inconsistent, and a definitive conclusion has yet to be reached regarding whether BB SOA yield and its overall net radiative forcing are

significant.^{1,2,7} Multiple studies, including newly developed SOA parametrization for laboratory studies, show that SOA contributions have been both grossly overestimated and underestimated in biomass burning models when compared to ambient observations.^{1–3,5–7}

The identities of the plants and ecosystems that burn influence the classes of BrC chromophores produced and overall BrC atmospheric lifetime from BB.^{1,3,6} BrC chromophores may persist longer in the environment than previously considered and could indicate that BrC aerosol has a larger positive radiative forcing contribution than originally anticipated.^{1,3,6} Therefore, to decrease the uncertainty from OA in climate modeling, numerous studies have requested that work be conducted in determining individual BrC chromophore identity, including BrC chromophores that range in polarity, aging effects, and BB source identity.^{1,3,8} In response to the fact that BB source-type affects emissions, a 2019 study updated

Received: April 14, 2020 Revised: June 3, 2020 Accepted: June 8, 2020 Published: June 8, 2020



emission factors and specific compound identification from various types of BB. That study found that gas-phase biacetyl (2,3-butanedione; BA) is a product of multiple anthropogenic and biogenic BB sources. The photooxidation of volatile organic compounds, including various methylated benzenes, found in significant concentrations in urban areas from sources like BB, transportation exhaust, gasoline, and solvent evaporation, also results in high production of BA. Wang et al. identified BA as the major degradation product of the reaction of ozone with several unsaturated ketones found in the troposphere. The photooxidation from the product of the reaction of ozone with several unsaturated ketones found in the troposphere.

BA is a diketone and will readily undergo reactive uptake into aqueous droplets in the atmosphere; it has been observed in concentrations of up to tens of micromolar in urban fogs, clouds, rain, and mists. ^{10,12,14–17} Despite the presence of BA in the atmosphere as a result of both direct sources and atmospheric sinks, few studies exist to investigate its atmospheric reactivity and potential contribution to BrC formation. ¹⁸ The lifetime for aqueous BA photolysis has been measured to be 1–1.6 h at midday in North Carolina. ¹⁰ Kampf et al. studied the BA + ammonium sulfate (AS) system among a comprehensive analysis of different dicarbonyl + amine systems but did not determine any product structures for this system, and it was concluded that BA + AS may not contribute to BrC light absorption because no absorbance peaks were observed at wavelengths greater than 250 nm after 144 h of reaction. ¹⁸

BA is structurally similar to other small water-soluble difunctional carbonyl compounds like methylglyoxal (MGly), glyoxal (Gly), glycolaldehyde (GAld), and hydroxyacetone (HA). The aqueous reactions of these small carbonyl compounds with AS have been shown to result in BrC formation. ^{19–35} The Gly + AS and MGly + AS reactions have been given specific attention due to their abundance in the atmosphere and increased light absorbance compared to the other carbonyl + AS systems. 18,19,23,24,26,28,32-39 These studies included product identification of specific BrC chromophores and concluded that imine-containing oligomers and substituted aromatic N-heterocycles are mainly responsible for the observed increase in absorbance in the actinic region. 18,19,23,24,26,33,35,36 While the hydroxycarbonyl systems of GAld + AS and HA + AS were previously thought to be unable to form these N-heterocycles and, therefore, be less relevant to BrC formation, Grace et al. identified these species within the GAld + AS and HA + AS reaction systems.³⁵ Due to their comparable abundance in the atmosphere to Gly and MGly or their capability to dominate absorbance at specific wavelengths, 26 that study highlighted why a more extensive range of BrC precursors needs to be considered to eliminate error in modeling global radiative forcing.³⁵

Atmospheric condensed-phase concentrations of BA are approximately an order of magnitude lower than Gly and MGly and are similar to GAld and HA, 14,15,17 and the BA + AS system will likely undergo similar Maillard-type browning reactions. BA can self-react to form aldol and acetal dimers and trimers, 40-42 and it is reasonable to assume that the important reaction pathways identified in previously studied carbonyl + AS systems could produce analogous BrC products in the BA + AS system. Although the ketone functional groups make this reaction less favorable than the analogous reaction with an aldehyde, imine formation is possible, as was observed in the HA + AS and MGly + AS reaction systems. Key structural features of products in the BA + AS system and its reaction

kinetics were identified using a combination of experimental methods. Theoretical methods accompanied these experiments to extract relevant absorption information for the individual identified products.

■ MATERIALS AND METHODS

Reagents. Biacetyl (2,3-butanedione; 99%) was obtained from Alfa Aesar, and ammonium sulfate was purchased from Sigma-Aldrich. For the isotopic substitution experiments, ¹⁵N-AS (99%) was purchased from Cambridge Isotope Laboratories, Inc. Food grade carbon dioxide was obtained from Airgas, while methanol (Optima LC/MS grade) and formic acid (Optima LC/MS grade) were purchased from Fisher Chemical.

Preparation of BA + AS Standards. Separate standard solutions of 1 M each of BA, AS, and $^{15}\text{N-AS}$ and a 3.5 M AS solution were prepared in Millipore Milli-Q Ultrapure water (Milli-Q, 18.2 M Ω cm resistivity). All standard solutions were used within 1 month of preparation.

SFC-MS/MS. Solutions analyzed using supercritical fluid chromatography-tandem mass spectrometry (SFC-MS/MS) contained 50 mM BA + 50 mM AS and were aged for 8 days under dark conditions at room temperature. Analogous sets of 50 mM BA + 50 mM ¹⁵N-AS were prepared for the isotopic substitution experiments. Samples were analyzed using a Waters ACQUITY Ultra Performance Chromatography (UPC²) supercritical fluid chromatography system coupled to a Waters XEVO TQD tandem quadrupole mass spectrometer. This technique is described in detail by Grace et al.⁴³ A binary gradient of CO₂ and methanol was used for elution of all samples through a Viridis UPC² BEH column $(3.0 \times 100 \text{ mm}, 1.7 \mu\text{m} \text{ particles})$. Starting conditions of 99% CO₂ and 1% methanol were held for 2 min and then the modifier content was increased to 17% until 15 min. The modifier content was increased again to 45% until 20 min and held until 26 min before the system returned to initial conditions for 4 min. The total flow rate was held constant at 1.0 mL/min with 0.25 mL/min MeOH + 1% formic acid makeup flow. The UPC² system back pressure was set to 1500 psi for the duration of all sample runs. Positive mode ESI conditions were set as follows: capillary voltage = 1.18 kV, cone voltage = 30 V, desolvation temperature = 250 °C, desolvation gas flow = 650 L/h, and cone flow = 1 L/h. Once a mass was identified in the mass spectrum, the sample was reanalyzed using extracted ion chromatography (EIC) to provide better sensitivity. Tandem mass spectrometry (fragmentation voltage = 20 eV) was also utilized to determine structural features.

Kinetic Experiments. A Cary 300 spectrophotometer was used to measure the absorbance of aqueous BA + AS samples blanked against a background of Milli-Q water. Three sets of reaction conditions were tested; 10, 25, and 50 mM BA were individually reacted with 3 M AS to be consistent with the high inorganic content of aqueous atmospheric aerosol. A constant volume of 800 μ L of solution was added to a 2 mm path length quartz cuvette (Starna Cells). The absorbance of the solution was collected over the range of 190–600 nm every 2 min for 48 h in a temperature-controlled cuvette holder maintained at 18 °C. The observed mass losses for the BA + AS solutions were comparable to the blank. After 48 h, an aliquot of the aqueous solution was diluted by a factor of 1:10 v/v in acetonitrile to precipitate the AS from solution and analyzed via SFC-MS/MS, as discussed above.

Figure 1. Self-reactions of BA to form aldol and acetal oligomers, along with a furanone $(m/z \ 199)$ and quinone $(m/z \ 137)$. Quinone formation was only observed in the presence of AS. Identified products are labeled with their observed m/z value $([M + H]^+)$.

Kinetics were inferred from time-resolved absorbance data in a similar fashion to those described in Fan et al. 44 In brief, spectra were decomposed into three Gaussian lineshapes that collectively represent their major peaks and geometries, fitted to observations using MATLAB (Mathworks, 2019b):

$$MAC(\lambda, t) \approx \sum_{i}^{3} \left[M_{c,i} + M_{i} \left(1 - \exp \left(-\frac{t}{M_{\tau,i}^{I}} \right) \right) \right]$$
$$\exp \left(-\left(\frac{\lambda - c_{i}}{\sigma_{i}} \right)^{2} \right)$$
(1)

Each Gaussian line shape contains a constant peak location, c, and spread, σ_{ij} and magnitudes that increases from an initial value, $M_{c,ij}$ by an offset value, M_{ij} via first-order kinetics with a time constant, $M_{\tau,i}^{\rm I}$. The mass absorbance coefficient, MAC(λ , t), normalizes absorbance data across different initial organic concentrations, $C_{\rm BA}^{\rm O}$, for mimic solutions with organic molecular weight, MW_{BA}, and measurement path length, l:

$$MAC(\lambda) = \frac{A(\lambda) \ln 10}{lC_{BA}^{O}MW_{BA}}$$
(2)

In representing spectra as multiple time-dependent functions, rate constants may be inferred for each major peak, enabling a separation of kinetic information for different potential chromophores contributing to a single dark chemistry system. Rate constants, $k^{\rm I}$, were calculated assuming first-order kinetics and constant, excess concentration of NH₄⁺ ions compared to organic concentration, which has been employed in several studies exploring water-soluble, carbonyl-containing organics: 22,44,45

$$k^{\rm I} = \frac{1}{[{\rm NH_4}^+]M_{\tau,i}^{\rm I}} \tag{3}$$

Here, the concentration of $\mathrm{NH_4}^+$ is set to 6 M. The maximum absorbance wavelengths of the previously mentioned computational estimations for potential chromophoric species were

then matched against the fitted line shape peaks from the decomposed spectra. The highest contributing species or family of species that absorbed at each wavelength were assigned inferred rate constants, accordingly. An aerosol will have solution nonidealities (i.e., inorganic activity coefficients) that are not captured by bulk mimic solution studies, and as a result, the inferred rate constants are lower bound estimates. As in similar kinetic analyses on carbonyl-containing reaction systems, 21,22,24,45-49 these inferred rate constants encapsulate entire suites of reactions, rather than individual steps in the mechanism. As these isolated mechanistic steps cannot be meaningfully decoupled from the overall reaction and are handled as a composite reaction, the bulk reaction rate of BA to form dark chemistry products is treated as effectively firstorder. While these are not rate constants in the strict sense of the term, they nonetheless provide rate-based kinetic information for these reaction systems in a comparable fashion. The first-order dependence with respect to NH₄⁺ concentration has also been applied in these same previous studies. 22,45,46,48

Computational Methodology. Density functional theory calculations were performed at the wB97X-D^{50,51}/6-311G(2d, p)^{52,53} level of theory using Gaussian 16⁵⁴ for all proposed BA + AS products following the procedure reported by Grace et al.³⁵ The procedure included ground state optimization of each compound and vibrational frequency calculations that confirmed all optimized geometries were at an energy minimum. The 15 lowest-lying excitations were calculated for each compound using time-dependent density functional theory (TDDFT). The excitation energies were also calculated using the CAM-B3LYP functional for comparison.⁵⁵ All calculations employed a conductor-like polarizable continuum model (CPCM) with water as the solvent. 56,57 The bright excitations for most of the compounds were overestimated, so a -0.6 eV shift was applied to calculated spectra in order to compare directly to experiment. The applied -0.6 eV red-shift takes into account overestimation of excitation energies by the exchange-correlation functionals, as well as average effects from the explicit solvent environment, and was found to provide

Figure 2. Nitrogen-containing compounds observed in the BA + AS system. Identified products are labeled with their observed m/z value ($M = \frac{1}{2} M + \frac{1}{2}$ H^{\uparrow}).

reasonable agreement with experiment in this study and in previous work.35 The applied red-shift does not take into account explicit solvent-solute interactions, and further discussion on the effect of explicit solvent molecules on spectral shifts is provided in the SI. A simulated absorption spectrum was constructed for each compound by applying a Gaussian broadening function to each excitation, using the default standard deviation of 0.4 eV as in GaussView 6.58 Natural transition orbitals (NTOs) and molecular orbitals (MOs) were visualized using GaussView (isosurface value: 0.02).

RESULTS AND DISCUSSION

All products identified in this study were observed in both the 8-day aged 50 mM BA + 50 mM AS samples and the 48-h aged samples containing BA + 3 M AS; proposed structures can be found in Figures 1 and 2 and Table S1.

Product Identification. BA (m/z 87) oligomerizes to produce dimers and trimers (Figures 1 and 2), like the previously mentioned carbonyl + AS systems. 40-42 Typical of carbonyl oligomerization reactions, BA readily forms aldol

dimers (m/z 173) via the corresponding enol. ^{40,59} The EIC for m/z 173 showed the presence of two isomers, which are likely to be the cyclic and open-chain forms of the dimer (Figure S1). The cyclic hemiacetal form of m/z 173 can react with hydrated BA to form trimers (Figure 2); 41,42 however, no trimers were observed via SFC-MS/MS. The trimer in Figure 1 can react with additional BA to produce a substituted furanone dimer (m/z 199). Fragmentation data for m/z 199 aligns with known fragmentation for methylated furanones, further supporting this assignment.⁶⁰ The decrease in pH over the course of the kinetics experiments supports the formation of acetic acid (Table 1), which has a mass too small to be observed by the MS.

From the open-chain form of m/z 173, dehydration results in the formation of m/z 155, which then reacts through two different aldol condensation pathways to yield different products. The first enol intermediate from the pathway (shown to the right of m/z 155 in Figure 1) can either (1) react with another molecule of BA and lose water to produce another open-chain oligomer (m/z 223) or (2) cyclize and lose water to form 2,5-dimethyl-1,4-benzoquinone (m/z 137).

Table 1. pH before and after 48 h of Reaction for BA + 3 M AS Systems^a

BA concentration (mM)	initial pH	final pH
50	4.72 ± 0.09	4.16 ± 0.02
25	5.09 ± 0.07	4.33 ± 0.07
10	5.47 ± 0.08	4.68 ± 0.02
all samples	5.14 ± 0.32	4.42 ± 0.12
^a Reported error is 1σ .		

Notably, m/z 137 is only seen in the BA + AS system and not in reactions when only BA is present, suggesting that quinone formation requires acid catalysis supplied by the ammonium ions in this system.⁶¹ In previous studies, 2,5-dimethyl-1,4-benzoquinone was shown to form as an aldol condensation dimer of BA but only in aqueous alkaline solutions.⁶² Fragmentation comparison to a standard (\geq 98%, Sigma-Aldrich) supports the structure of m/z 137 (Figure S2). The presence of a quinone is significant to note, as quinones are unique to the BA + AS system compared to the products identified in the other carbonyl + AS systems mentioned above. All proposed structures shown in Figure 1 were further supported by ¹⁵N-AS experiments (i.e., no nitrogens were present in the structures). Fragmentation information is provided in Table S1.

As shown in Figure 2, incorporation of imines and amines into the BA oligomers enables the formation of substituted imidazoles (m/z 111, 197), oxazoles (m/z 112, 154, 172, 198,302), a pyrrole (m/z 198), and aliphatic N-containing heterocycles (m/z 172, 240, 258). Larger, N-containing oligomers in the BA + AS system (e.g., multiple isomers of m/z 258; Figure S3) react with water to produce Schiff bases and hydrates, thus enabling the cleavage of acetic acid and subsequent elimination to produce a substituted imidazole, oxazole, or pyrrole (m/z 197, m/z 198, and m/z 198,respectively). Similar reaction series were proposed by Yu et al. for imidazole formation in the Gly + AS system and by De Haan et al. for methylimidazole formation in the MGly + AS system. 23,24 Acetic acid production during oxazole, imidazole, and pyrrole formation could also contribute to the observed decrease in the system pH over time (Table 1).

From m/z 198, either (1) subsequent hydration and oligomerization with another BA can produce further substituted oxazoles (m/z 302) or (2) reactions with NH₃ and BA can produce an intermediate capable of forming another Schiff base that subsequently undergoes fragmentation and water loss, resulting in additional oxazole derivatives (m/z112, 154, 172). An analogous reaction pathway to m/z 197 produces 2,4,5-trimethylimidazole (m/z 111). An alternate reaction pathway to trimethyl- oxazole and imidazole formation can be found in Figure S4. Kampf et al. previously identified a strong ESI-MS signal at m/z 112, but this mass was not attributed to trimethyloxazole. 18 However, the reported m/z, sum formula, and fragmentation data match that of this study, 18 and a standard prepared using 2,4,5-trimethyloxazole (95%, Sigma-Aldrich) further confirmed the validity of this identification method. All oxazole derivatives were found to elute earlier on the column than their analogous imidazole derivatives (Figure S1). Furthermore, the substituted oxazoles and imidazoles exhibited fragmentation behavior consistent with that of the trimethyloxazole standard or imidazole and substituted imidazole standards used previously by Grace et al.35 Notably, it was previously thought that imidazole

formation would not be possible due to competing trimeric cyclic acetal formation.¹⁸ However, introducing nitrogens during trimer production enables imidazole formation to occur through Schiff base intermediates, as shown in Figure 2. Isotopic substitution experiments using ¹⁵N-AS confirm the nitrogen(s) in all structures reported in Figure 2.

The reduced reactivity of the ketone carbonyls in BA compared to the aldehydes found in MGly, Gly, and GAld may influence the classes of products formed. The presence of the α -diketone in BA leads to a decreased number of imidazole derivatives and an increased presence of oxazole derivatives compared to other carbonyl + AS systems. ^{28,35} Additionally, no pyrazines were identified in the BA + AS system. While BA can react with glycine to form tetramethylpyrazine, its reaction with AS does not favorably produce a species able to reduce the imine-substituted BA (m/z 86) needed for pyrazine formation. ⁶³

Light Absorbance. The reacted BA + AS system exhibits light absorbance similar to that of other small carbonyls, ⁴⁴ with absorbance peaks at approximately 190, 224, and 280 nm. An example of the empirical spectral decomposition of the BA + AS spectra across multiple time points is shown in Figure 3.

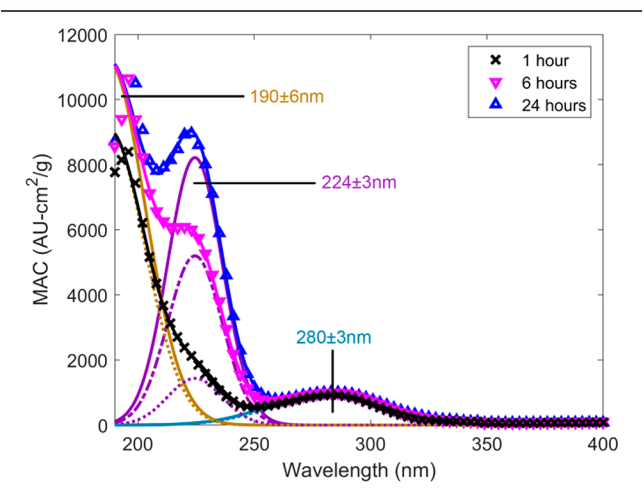


Figure 3. Observed mass absorbance coefficient (MAC) for 50 mM BA + 3 M AS (points) and approximated MAC values using a three-curve Gaussian decomposition (lines).

Complete spectral decomposition results, aggregated by concentration, can be found in Figure S5. Across all concentrations tested, the three Gaussian lineshapes were found to converge as one slowly increasing peak at 224 \pm 3 nm, with two quickly converging peaks at 280 \pm 3 and 190 \pm 6 nm. There is little to no statistical difference in inferred locations for the peaks at 190 and 224 nm with respect to BA concentration (p = 0.104 and 0.282, respectively). A statistically significant (p = 0.015) dependence with respect to BA concentration was observed for the location of the peak at 280 nm, slightly red-shifting as BA concentration increases, from 278 nm for 10 mM samples to 282 nm at 50 mM. However, as this method cannot definitively identify individual chromophores that may be contributing to this slight shift, combined with the relative variation in fitted peak location, little additional information can be inferred from this observed shift.

Inferred lower-bound first-order rate constants, calculated via eq 3, are summarized in Figure 4 and Table S2. These rate constants inferred for the BA + AS system are comparable in

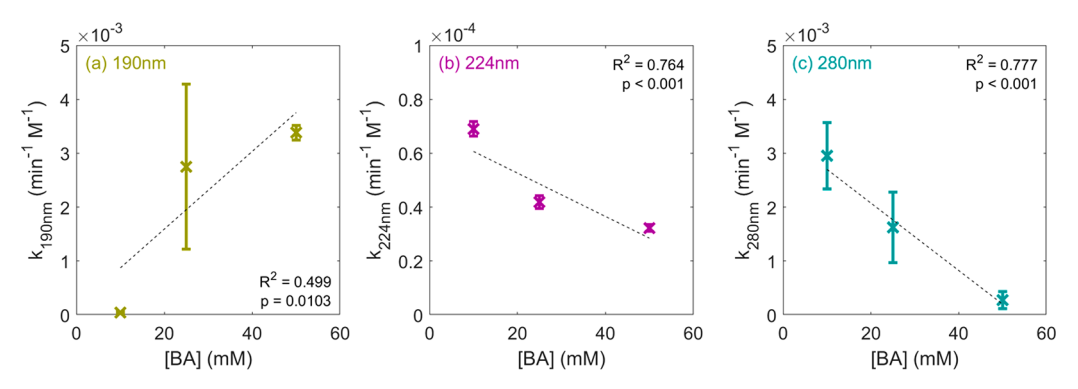


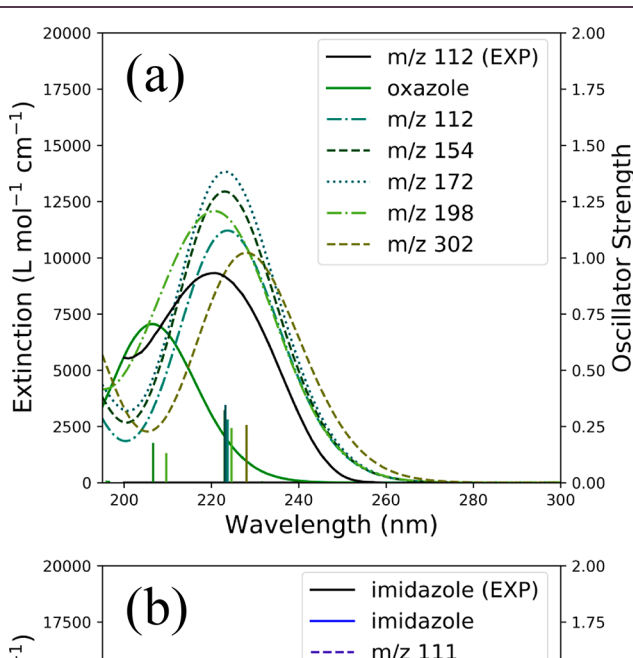
Figure 4. Inferred lower-bound first-order rate constants for decomposed absorbance peaks by location. Peak locations were estimated to be (a) 190 ± 6 , (b) 224 ± 3 , and (c) 280 ± 3 nm.

magnitude to values calculated from similar carbonyl + AS solutions using this method, which ranged from 2×10^{-4} to 5 $\times 10^{-3} \,\mathrm{M}^{-1} \,\mathrm{min}^{-1}$ for lineshapes within the GAld + AS, Gly + AS, and MGly + AS reaction systems. 44 The inferred rates for all three fitted lineshapes demonstrate statistically significant concentration dependence, as seen in Figure 4. Inferred rate of formation at 280 nm was observed to slow as BA concentrations increased, while increases in the 190 nm region accelerated with BA concentration. The peaks at 190 and 280 nm exhibit comparable rates of formation, ranging across modeled concentrations from $4.1(\pm 1.7) \times 10^{-5}$ to $3.3(\pm 0.1)$ $\times 10^{-3} \text{ M}^{-1} \text{ min}^{-1}$ and from $2.7(\pm 1.6) \times 10^{-4}$ to $2.9(\pm 0.6) \times 10^{-4}$ 10⁻³ M⁻¹ min⁻¹, respectively. Both peaks achieve nominally steady MAC values within approximately 12 h of solution aging and demonstrate relatively small changes in magnitude of absolute MAC over the observed time frame. This small shift implies that, while the relevant chemistry in these wavelengths occurs quickly, the total absorbance contribution of evolved chromophores is somewhat small.

While averaging nearly 2 orders of magnitude slower than the other two lineshapes, ranging from $3.2(\pm0.1)\times10^{-5}$ to $6.9(\pm0.3)\times10^{-5}$ M $^{-1}$ min $^{-1}$ across modeled concentrations, the peak at 224 nm demonstrated the largest change in overall peak intensity, indicating formation of significant chromophoric products in this region, as discussed below. Like the peak at 280 nm, the increase in light absorbance over time slowed as organic concentration increased; however, this concentration dependence is relatively smaller by comparison, staying within less than an order of magnitude over the concentration ranges tested.

Many of the identified compounds were shown via TDDFT calculations to absorb light in the 190 nm range (Figures S6 and S7), including imidazoles, oxazoles, a quinone, a pyrrole, and several open chain oligomers. While monitoring this peak is useful for determining reaction progress, the observed peaks at 224 and 280 nm offer more insight into the composition of the reacted mixture. The identified oxazole, imidazole, and pyrrole derivatives all have calculated absorbance values near 220 nm (Figures 5 and S6), suggesting that a significant portion of the chromophoric reaction products in this mixture are oxazoles, imidazoles, and pyrroles.

TDDFT calculations show that imidazole and oxazole exhibit similar low-lying excitations that result in absorption maxima centered around 190–200 nm. Natural transition orbitals for the excitations in oxazoles, imidazoles, and pyrroles were analyzed and are provided in the Supporting Information (Figures S11–S25). In imidazole and oxazole, the first



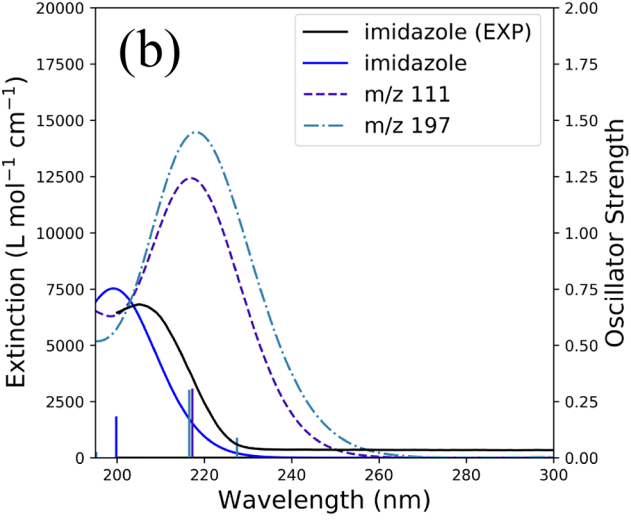


Figure 5. Calculated absorption spectra (left y axis) for aromatic heterocycles with and without substituent groups for (a) oxazole and its identified derivatives in green and (b) imidazole and its identified derivatives in blue. The calculated vertical excitation energies are shown as sticks, with oscillator strengths corresponding to the right y axis. Calculated spectra are compared to spectra measured for relevant experimental standards (EXP). Experimental absorption intensity is provided in arbitrary units.

excitation is the $\pi-\pi^*$ transition, which has a large oscillator strength (i.e., absorption intensity) compared to other low-

lying transitions. The excitation energy for this lowest-lying $\pi-\pi^*$ transition is lower in oxazoles than imidazoles. The second excitation is the $n-\pi^*$ transition from the nitrogen and/or oxygen nonbonding p-electrons to the heterocycle π^* orbital, and the third excitation is a $\pi-\pi^*$ transition. The relative energy of the second $\pi-\pi^*$ transition is higher in oxazole than imidazole, which results in two distinct absorption maxima in the calculated spectra for oxazole, compared to a single broad peak for imidazole.

The addition of a substituent group red-shifts the absorption maxima of these characteristic excitations with respect to oxazole and imidazole, as shown in the spectra for the observed substituted oxazole compounds (m/z 112, 154, 172, 198, 302; Figure 5a). When carbonyl moieties are present in the substituent groups, additional low-lying excitations appear in the spectrum. For instance, in the case of m/z 154, the first excitation is the $n-\pi^*$ transition localized on the substituent carbonyl, and the second is a charge transfer transition between the heterocycle-localized π orbital to the carbonyllocalized π^* orbital. As a result, these transitions have small oscillator strength and do not significantly red-shift the overall absorption spectrum. However, with much larger substituent groups containing a carbonyl, the orbitals become more delocalized across the molecule, resulting in red-shifted excitation energies for transitions involving the carbonyl as well as increased absorption intensity. For example, in the similar imidazole, pyrrole, and oxazole compounds (i.e., m/z197, 198, 198) the carbonyl π^* orbital becomes more delocalized, which decreases the charge transfer character of the transition between heterocycle π orbital and carbonyl π^* orbital and increases the oscillator strength of the transition so that it contributes to the overall spectrum. In both the imidazole derivative (m/z 197) and the pyrrole derivative (m/z 198), this charge transfer excitation energy is lower than the heterocycle $\pi - \pi^*$ excitation, as shown in Table S3.

Two of the identified fused heterocycles are predicted to absorb in the region between the 224 and 280 nm peaks, with excitation wavelengths of 247 (m/z 240) and 237 nm (m/z 258). These fused heterocycles contain a carbon–carbon double bond and at least one carbonyl moiety. The presence of the carbonyl groups results in low-lying $n-\pi^*$ transitions between the nonbonding oxygen orbitals and the carbonyl-localized π^* orbital. These are symmetry-forbidden excitations which have little to no oscillator strength and do not contribute greatly to the overall absorption spectrum. The strongly absorbing excitation is the $\pi-\pi^*$ transition of the heterocycle double bond, which is delocalized across the carbonyl moieties.

For the fused heterocycles that contain a carbon–nitrogen double bond, the protonation state of the nitrogen can have a significant effect on the absorption energy (Figure S7). Exact pK_a values are difficult to predict for these previously unidentified compounds, but m/z 240 and 258 are likely to be protonated under these pH conditions due to their similarity to other compounds with pK_a values in the range of 2.5–6.0. In the case of these fused heterocycles, when the nitrogen is deprotonated, the absorption maximum is closer to the 224 nm peak, but when the nitrogen is protonated, the absorption maximum is red-shifted closer to the 280 nm peak, suggesting that these compounds could contribute to either absorbance peak depending on their protonation state. The remaining N-containing species, excluding the oxazoles and pyrrole, are expected to be

protonated under these pH conditions when compared to structurally similar compounds with pK_a values in the range of 4.5–9.0.^{64,65} However, protonation has minor effects on the strongly absorbing excitations of these compounds and does not result in significant spectral shifts (Figure S7).

The slight increase in light absorbance with solution age observed at 280 nm is attributed to formation of 2,5-dimethyl-1,4-benzoquinone (m/z 137). The quinone excitations consist of multiple low-lying transitions that are symmetry forbidden and thus have little to no oscillator strength and do not contribute significantly to the absorption spectrum. The first two excitations for m/z 137 are the $n-\pi^*$ transition involving the carbonyl-localized nonbonding p-electrons and the quinone-localized π^* orbital. The third excitation is the low-lying symmetry forbidden $\pi-\pi^*$ transition localized on the quinone, and the fourth excitation is the symmetry-allowed, strongly absorbing $\pi-\pi^*$ transition (277 nm), also localized on the quinone.

The increased absorbance in the 280 nm region can also be attributed to the formation of the furanone derivative (m/z)199) and open chain oligomers (m/z 155, 223). Similar to the quinone derivative, the furanone derivative and the open chain oligomers contain multiple carbonyl moieties, and thus their absorption spectra also include multiple low-lying excitations that involve carbonyl $n-\pi^*$ transitions. These excitations have little to no oscillator strength and do not contribute significantly to the overall spectrum. The π - π * transitions in these compounds contribute to absorption that tails into the actinic region. For the furanone derivative, the π - π * transition with a large oscillator strength is predicted at about 270 nm, slightly higher in energy than the 280 nm peak. For the open chain oligomers, the π - π * transition with a large oscillator strength is predicted in the vicinity of 300 nm, slightly lower in energy than the 280 nm peak.

CONCLUSIONS

BA reacts with AS to produce open chain oligomers and heterocycles, similar to those observed in other carbonyl + AS reaction systems. ^{28,35} However, the presence of the α -diketone in BA leads to an increase in the number of oxazole compounds formed when compared to analogous systems containing similar small α -dicarbonyl and α -hydroxycarbonyl compounds (i.e., MGly, Gly, GAld, and HA) and a decrease in the number of imidazole compounds and pyrazines. 28,35,36 Reaction pathways to produce the quinone are also more accessible for this α -diketone than the other carbonyl + AS systems. Kampf et al. observed no absorbance at wavelengths greater than 250 nm in solutions containing reacted 1 M BA + 1 M AS and concluded that BA + AS does not contribute to BrC.¹⁸ However, the peak observed at 280 nm in this work shows that BA + AS can exhibit tailing absorption in the actinic region (λ >300 nm), ¹⁸ analogous to the Gly + AS and HA + AS BrC systems. This indicates that BA + AS could be classified as a BrC contributor in the same way as these carbonyl + AS systems. 24,35,44

Photolysis rate constants inferred from the aqueous BA half-lives measured by Faust et al. are on comparable orders of magnitude to the dark chemistry reactions modeled in this work. Therefore, while photolysis will contribute to a loss of BA under irradiated (daytime) conditions, the dark chemistry reactions that are occurring in parallel (with or without incident radiation) are likely to participate to a relevant degree.

Thus, studying the dark chemistry reactions is important for understanding how BA + AS chemistry affects radiative forcing.

As previously stated, urban atmospheric condensed-phase BA concentrations are approximately an order of magnitude lower than those of Gly and MGly and are similar to those of GAld and HA. 14,15,17 Therefore, while the products identified herein are likely to form in smaller quantities than the products of Gly and MGly with AS, they form at the same rates as the products of GAld and HA with AS and therefore are likely to be found in similar quantities. In addition, the presence of BA in the condensed-phase and its ability to react to form substituted heterocyclic compounds opens up the possibility of cross-reactions between other carbonyls in the complex mixtures found in aqueous atmospheric aerosol and may shift the product formation toward oxazole formation, changing the products formed. 18,45 Further oligomerization by cross reactions of other compounds found in aqueous cloud or aerosol droplets could red-shift the absorbance into the actinic region.

MGly and its dark chemistry reaction products have been observed to be surface-active, ^{22,39} and it is possible that the additional methylation in BA will result in its analogous reaction system being surface-active as well. However, there is currently a lack of surface activity information for the BA + AS reaction system, and this analysis must therefore assume that the relevant dark chemistry reactions are uniformly occurring within the condensed-phase. More studies are necessary to determine how BA-dependent interfacial phenomena will affect aerosol systems, and gaining an understanding of bulk BA + AS behavior is an important step toward this goal. This system could also contribute another pathway for aqueous condensedphase reactions from gas-phase BB emissions, providing another link between BB and aged SOA. Improved understanding of BrC sources from BB can help guide future studies probing more complex reaction systems in order to achieve better accuracy when factoring these emissions into global climate models.

ASSOCIATED CONTENT

Supporting Information

The Supporting Information is available free of charge at https://pubs.acs.org/doi/10.1021/acsearthspace-chem.0c00096.

Extracted ion chromatograms, structures, and fragmentation information for all identified products; complete spectral decomposition and kinetics results of UV—visible absorbance spectra, aggregated by concentration; calculated UV—visible absorption data for all identified products and selected protonated products; discussion on the effect of explicit solvent on calculated absorption data; calculated UV—visible absorption data compared to experimental standards; natural transition orbitals for identified products predicted to contribute to the experimental absorption spectra (PDF)

AUTHOR INFORMATION

Corresponding Author

Melissa M. Galloway — Department of Chemistry, Lafayette College, Easton, Pennsylvania 18042, United States of America; orcid.org/0000-0002-8518-1888; Phone: (610)330-5206; Email: gallowam@lafayette.edu; Fax: (610)330-5714

Authors

Daisy N. Grace — Department of Chemistry, Lafayette College, Easton, Pennsylvania 18042, United States of America; o orcid.org/0000-0002-1088-9267

Emily N. Lugos – Department of Chemistry, Lafayette College, Easton, Pennsylvania 18042, United States of America

Shiqing Ma — Department of Chemical and Biomolecular Engineering, Lafayette College, Easton, Pennsylvania 18042, United States of America

Daniel R. Griffith — Department of Chemistry, Lafayette College, Easton, Pennsylvania 18042, United States of America; orcid.org/0000-0002-0361-8290

Heidi P. Hendrickson — Department of Chemistry, Lafayette College, Easton, Pennsylvania 18042, United States of America; orcid.org/0000-0002-5012-738X

Joseph L. Woo — Department of Chemical and Biomolecular Engineering, Lafayette College, Easton, Pennsylvania 18042, United States of America; orcid.org/0000-0001-7264-3425

Complete contact information is available at: https://pubs.acs.org/10.1021/acsearthspacechem.0c00096

Author Contributions

The manuscript was written through contributions of all authors. All authors have given approval to the final version of the manuscript.

Notes

The authors declare no competing financial interest.

ACKNOWLEDGMENTS

Funding for this work was provided by the National Science Foundation (MRI-1626100). Computational resources were provided in part by the MERCURY consortium (http://mercuryconsortium.org/) under NSF Grants CHE-1229354 and CHE-1662030. E.N.L. and H.P.H. thank Prof. Chun Wai Liew at Lafayette College for computational support. The authors also thank Sierra J. Cole for her assistance in experimental setup and manuscript insight.

REFERENCES

- (1) Lim, C. Y.; Hagan, D. H.; Coggon, M. M.; Koss, A. R.; Sekimoto, K.; de Gouw, J.; Warneke, C.; Cappa, C. D.; Kroll, J. H. Secondary organic aerosol formation from the laboratory oxidation of biomass burning emissions. *Atmos. Chem. Phys.* **2019**, *19* (19), 12797–12809.
- (2) Carter, T. S.; Heald, C. L.; Jimenez, J. L.; Campuzano-Jost, P.; Kondo, Y.; Moteki, N.; Schwarz, J. P.; Wiedinmyer, C.; Darmenov, A. S.; da Silva, A. M.; Kaiser, J. W. How emissions uncertainty influences the distribution and radiative impacts of smoke from fires in North America. *Atmos. Chem. Phys.* **2020**, *20* (4), 2073–2097.
- (3) Fleming, L. T.; Lin, P.; Roberts, J. M.; Selimovic, V.; Yokelson, R.; Laskin, J.; Laskin, A.; Nizkorodov, S. A. Molecular composition and photochemical lifetimes of brown carbon chromophores in biomass burning organic aerosol. *Atmos. Chem. Phys.* **2020**, *20* (2), 1105–1129.
- (4) IPCC Climate Change 2013: The Physical Science Basis. Contribution of Working Group I to the Fifth Assessment Report of the Intergovernmental Panel on Climate Change; Cambridge University Press: Cambridge, U.K., 2013.
- (5) Wang, X.; Heald, C. L.; Ridley, D. A.; Schwarz, J. P.; Spackman, J. R.; Perring, A. E.; Coe, H.; Liu, D.; Clarke, A. D. Exploiting simultaneous observational constraints on mass and absorption to estimate the global direct radiative forcing of black carbon and brown carbon. *Atmos. Chem. Phys.* **2014**, *14* (20), 10989–11010.
- (6) Ahern, A. T.; Robinson, E. S.; Tkacik, D. S.; Saleh, R.; Hatch, L. E.; Barsanti, K. C.; Stockwell, C. E.; Yokelson, R. J.; Presto, A. A.;

- Robinson, A. L.; Sullivan, R. C.; Donahue, N. M. Production of Secondary Organic Aerosol During Aging of Biomass Burning Smoke From Fresh Fuels and Its Relationship to VOC Precursors. *J. Geophys. Res.: Atmos.* **2019**, *124* (6), 3583–3606.
- (7) Pan, X.; Ichoku, C.; Chin, M.; Bian, H.; Darmenov, A.; Colarco, P.; Ellison, L.; Kucsera, T.; da Silva, A.; Wang, J.; Oda, T.; Cui, G. Six global biomass burning emission datasets: intercomparison and application in one global aerosol model. *Atmos. Chem. Phys.* **2020**, 20 (2), 969–994.
- (8) Tang, J.; Li, J.; Su, T.; Han, Y.; Mo, Y.; Jiang, H.; Cui, M.; Jiang, B.; Chen, Y.; Tang, J.; Song, J.; Peng, P.; Zhang, G. Molecular compositions and optical properties of dissolved brown carbon in biomass burning, coal combustion, and vehicle emission aerosols illuminated by excitation—emission matrix spectroscopy and Fourier transform ion cyclotron resonance mass spectrometry analysis. *Atmos. Chem. Phys.* **2020**, 20 (4), 2513–2532.
- (9) Andreae, M. O. Emission of trace gases and aerosols from biomass burning an updated assessment. *Atmos. Chem. Phys.* **2019**, 19 (13), 8523–8546.
- (10) Faust, B. C.; Powell, K.; Rao, C. J.; Anastasio, C. Aqueous-phase photolysis of biacetyl (An α -dicarbonyl compound): A sink for biacetyl, and a source of acetic acid, peroxyacetic acid, hydrogen peroxide, and the highly oxidizing acetylperoxyl radical in aqueous aerosols, fogs, and clouds. *Atmos. Environ.* **1997**, 31 (3), 497–510.
- (11) Luo, H.; Jia, L.; Wan, Q.; An, T.; Wang, Y. Role of liquid water in the formation of O₃ and SOA particles from 1,2,3-trimethylbenzene. *Atmos. Environ.* **2019**, 217, 116955.
- (12) Zhang, P.; Huang, J.; Shu, J.; Yang, B. Comparison of secondary organic aerosol (SOA) formation during *o-, m-,* and *p-xylene* photooxidation. *Environ. Pollut.* **2019**, 245, 20–28.
- (13) Wang, X.; Sun, J.; Bao, L.; Mei, Q.; Wei, B.; An, Z.; Xie, J.; He, M. Mechanisms and Kinetic Parameters for the Gas-Phase Reactions of 3-Methyl-3-buten-2-one and 3-Methyl-3-penten-2-one with Ozone. *J. Phys. Chem. A* **2019**, 123 (13), 2745–2755.
- (14) Igawa, M.; Munger, J. W.; Hoffmann, M. R. Analysis of aldehydes in cloud- and fogwater samples by HPLC with a postcolumn reaction detector. *Environ. Sci. Technol.* **1989**, 23 (5), 556–561.
- (15) Munger, J. W.; Collett, J.; Daube, B.; Hoffmann, M. R. Fogwater chemistry at Riverside, California. *Atmos. Environ., Part B* **1990**, 24 (2), 185–205.
- (16) Munger, J. W.; Jacob, D. J.; Daube, B. C.; Horowitz, L. W.; Keene, W. C.; Heikes, B. G. Formaldehyde, glyoxal, and methylglyoxal in air and cloudwater at a rural mountain site in central Virginia. *J. Geophys. Res.* 1995, 100 (D5), 9325–9333.
- (17) van Pinxteren, D.; Plewka, A.; Hofmann, D.; Müller, K.; Kramberger, H.; Svrcina, B.; Bächmann, K.; Jaeschke, W.; Mertes, S.; Collett, J. L.; Herrmann, H. Schmücke hill cap cloud and valley stations aerosol characterisation during FEBUKO (II): Organic compounds. *Atmos. Environ.* **2005**, *39* (23), 4305–4320.
- (18) Kampf, C. J.; Filippi, A.; Zuth, C.; Hoffmann, T.; Opatz, T. Secondary brown carbon formation via the dicarbonyl imine pathway: nitrogen heterocycle formation and synergistic effects. *Phys. Chem. Chem. Phys.* **2016**, *18* (27), 18353–18364.
- (19) De Haan, D. O.; Corrigan, A. L.; Smith, K. W.; Stroik, D. R.; Turley, J. J.; Lee, F. E.; Tolbert, M. A.; Jimenez, J. L.; Cordova, K. E.; Ferrell, G. R. Secondary Organic Aerosol-Forming Reactions of Glyoxal with Amino Acids. *Environ. Sci. Technol.* **2009**, *43* (8), 2818–2824.
- (20) Galloway, M. M.; Chhabra, P. S.; Chan, A. W. H.; Surratt, J. D.; Flagan, R. C.; Seinfeld, J. H.; Keutsch, F. N. Glyoxal uptake on ammonium sulphate seed aerosol: reaction products and reversibility of uptake under dark and irradiated conditions. *Atmos. Chem. Phys.* **2009**, *9* (10), 3331–3345.
- (21) Shapiro, E. L.; Szprengiel, J.; Sareen, N.; Jen, C. N.; Giordano, M. R.; McNeill, V. F. Light-absorbing secondary organic material formed by glyoxal in aqueous aerosol mimics. *Atmos. Chem. Phys.* **2009**, 9 (7), 2289–2300.

- (22) Sareen, N.; Schwier, A. N.; Shapiro, E. L.; Mitroo, D.; McNeill, V. F. Secondary organic material formed by methylglyoxal in aqueous aerosol mimics. *Atmos. Chem. Phys.* **2010**, *10* (3), 997–1016.
- (23) De Haan, D. O.; Hawkins, L. N.; Kononenko, J. A.; Turley, J. J.; Corrigan, A. L.; Tolbert, M. A.; Jimenez, J. L. Formation of Nitrogen-Containing Oligomers by Methylglyoxal and Amines in Simulated Evaporating Cloud Droplets. *Environ. Sci. Technol.* **2011**, *45* (3), 984–991.
- (24) Yu, G.; Bayer, A. R.; Galloway, M. M.; Korshavn, K. J.; Fry, C. G.; Keutsch, F. N. Glyoxal in aqueous ammonium sulfate solutions: Products, kinetics and hydration effects. *Environ. Sci. Technol.* **2011**, 45 (15), 6336–6342.
- (25) Galloway, M. M.; Powelson, M. H.; Sedehi, N.; Wood, S. E.; Millage, K. D.; Kononenko, J. A.; Rynaski, A. D.; De Haan, D. O. Secondary Organic Aerosol Formation during Evaporation of Droplets Containing Atmospheric Aldehydes, Amines, and Ammonium Sulfate. *Environ. Sci. Technol.* **2014**, *48* (24), 14417–14425.
- (26) Powelson, M. H.; Espelien, B.; Hawkins, L. N.; Galloway, M. M.; De Haan, D. O. Brown carbon formation by aqueous-phase carbonyl compound reactions with amines and ammonium sulfate. *Environ. Sci. Technol.* **2014**, 48 (2), 985–993.
- (27) Laskin, A.; Laskin, J.; Nizkorodov, S. A. Chemistry of atmospheric brown carbon. *Chem. Rev.* **2015**, *115* (10), 4335–4382. (28) Lin, P.; Laskin, J.; Nizkorodov, S. A.; Laskin, A. Revealing Brown Carbon Chromophores Produced in Reactions of Methylglyoxal with Ammonium Sulfate. *Environ. Sci. Technol.* **2015**, *49* (24), 14257–14266.
- (29) McNeill, V. F. Aqueous Organic Chemistry in the Atmosphere: Sources and Chemical Processing of Organic Aerosols. *Environ. Sci. Technol.* **2015**, 49 (3), 1237–1244.
- (30) Hawkins, L. N.; Lemire, A. N.; Galloway, M. M.; Corrigan, A. L.; Turley, J. J.; Espelien, B. M.; De Haan, D. O. Maillard Chemistry in Clouds and Aqueous Aerosol As a Source of Atmospheric Humic-Like Substances. *Environ. Sci. Technol.* **2016**, *50* (14), 7443–7452.
- (31) Ackendorf, J. M.; Ippolito, M. G.; Galloway, M. M. pH Dependence of the Imidazole-2-carboxaldehyde Hydration Equilibrium: Implications for Atmospheric Light Absorbance. *Environ. Sci. Technol. Lett.* **2017**, *4* (12), 551–555.
- (32) De Haan, D. O.; Hawkins, L. N.; Welsh, H. G.; Pednekar, R.; Casar, J. R.; Pennington, E. A.; de Loera, A.; Jimenez, N. G.; Symons, M. A.; Zauscher, M.; Pajunoja, A.; Caponi, L.; Cazaunau, M.; Formenti, P.; Gratien, A.; Pangui, E.; Doussin, J.-F. Brown Carbon Production in Ammonium- or Amine-Containing Aerosol Particles by Reactive Uptake of Methylglyoxal and Photolytic Cloud Cycling. *Environ. Sci. Technol.* **2017**, *51* (13), 7458–7466.
- (33) Rodriguez, A. A.; de Loera, A.; Powelson, M. H.; Galloway, M. M.; De Haan, D. O. Formaldehyde and Acetaldehyde Increase Aqueous-Phase Production of Imidazoles in Methylglyoxal/Amine Mixtures: Quantifying a Secondary Organic Aerosol Formation Mechanism. *Environ. Sci. Technol. Lett.* **2017**, *4* (6), 234–239.
- (34) De Haan, D. O.; Tapavicza, E.; Riva, M.; Cui, T.; Surratt, J. D.; Smith, A. C.; Jordan, M.-C.; Nilakantan, S.; Almodovar, M.; Stewart, T. N.; de Loera, A.; De Haan, A. C.; Cazaunau, M.; Gratien, A.; Pangui, E.; Doussin, J.-F. Nitrogen-Containing, Light-Absorbing Oligomers Produced in Aerosol Particles Exposed to Methylglyoxal, Photolysis, and Cloud Cycling. *Environ. Sci. Technol.* **2018**, *52* (7), 4061–4071.
- (35) Grace, D. N.; Sharp, J. R.; Holappa, R. E.; Lugos, E. N.; Sebold, M. B.; Griffith, D. R.; Hendrickson, H. P.; Galloway, M. M. Heterocyclic Product Formation in Aqueous Brown Carbon Systems. *ACS Earth Space Chem.* **2019**, *3* (11), 2472–2481.
- (36) Hawkins, L. N.; Welsh, H. G.; Alexander, M. V. Evidence for pyrazine-based chromophores in cloud water mimics containing methylglyoxal and ammonium sulfate. *Atmos. Chem. Phys.* **2018**, *18* (16), 12413–12431.
- (37) Lee, A. K. Y.; Zhao, R.; Li, R.; Liggio, J.; Li, S.-M.; Abbatt, J. P. D. Formation of Light Absorbing Organo-Nitrogen Species from Evaporation of Droplets Containing Glyoxal and Ammonium Sulfate. *Environ. Sci. Technol.* **2013**, 47 (22), 12819–12826.

- (38) Sareen, N.; Moussa, S. G.; McNeill, V. F. Photochemical Aging of Light-Absorbing Secondary Organic Aerosol Material. *J. Phys. Chem. A* **2013**, *117* (14), 2987–2996.
- (39) Beier, T.; Cotter, E. R.; Galloway, M. M.; Woo, J. L. In Situ Surface Tension Measurements of Hanging Droplet Methylglyoxal/Ammonium Sulfate Aerosol Mimics under Photooxidative Conditions. ACS Earth Space Chem. 2019, 3 (7), 1208–1215.
- (40) Birch, A. J.; Moye, C. J. 75. Studies in relation to biosynthesis. Part X. A synthesis of lumichrome from non-benzenoid precursors. *J. Chem. Soc.* **1957**, No. 0, 412–414.
- (41) Cresswell, R. M.; Smith, W. R. D.; Wood, H. C. S. 960. The structure of two trimers of biacetyl. *J. Chem. Soc.* **1961**, No. 0, 4882–4885
- (42) Alexandropoulou, I.; Crabb, T. A.; Patel, A. V.; Hudec, J. Acid-promoted reactions of butan-2,3-dione. *Tetrahedron* **1999**, 55 (18), 5867–5874.
- (43) Grace, D. N.; Sebold, M. B.; Galloway, M. M. Separation and detection of aqueous atmospheric aerosol mimics using supercritical fluid chromatography—mass spectrometry. *Atmos. Meas. Tech.* **2019**, 12 (7), 3841–3851.
- (44) Fan, M.; Ma, S.; Ferdousi, N.; Dai, Z.; Woo, J. L. Modeling of Carbonyl/Ammonium Sulfate Aqueous Brown Carbon Chemistry via UV/Vis Spectral Decomposition. *Atmosphere* **2020**, *11* (4), 358.
- (45) Schwier, A. N.; Sareen, N.; Mitroo, D.; Shapiro, E. L.; McNeill, V. F. Glyoxal-Methylglyoxal Cross-Reactions in Secondary Organic Aerosol Formation. *Environ. Sci. Technol.* **2010**, *44* (16), 6174–6182.
- (46) Nozière, B.; Dziedzic, P.; Córdova, A. Products and Kinetics of the Liquid-Phase Reaction of Glyoxal Catalyzed by Ammonium Ions (NH₄⁺). *J. Phys. Chem. A* **2009**, *113* (1), 231–237.
- (47) Sedehi, N.; Takano, H.; Blasic, V. A.; Sullivan, K. A.; De Haan, D. O. Temperature- and pH-dependent aqueous-phase kinetics of the reactions of glyoxal and methylglyoxal with atmospheric amines and ammonium sulfate. *Atmos. Environ.* **2013**, *77*, 656–663.
- (48) Yi, Y.; Cao, Z.; Zhou, X.; Xue, L.; Wang, W. Formation of aqueous-phase secondary organic aerosols from glycolaldehyde and ammonium sulfate/amines: A kinetic and mechanistic study. *Atmos. Environ.* **2018**, *181*, 117–125.
- (49) Yi, Y.; Zhou, X.; Xue, L.; Wang, W. Air pollution: formation of brown, lighting-absorbing, secondary organic aerosols by reaction of hydroxyacetone and methylamine. *Environ. Chem. Lett.* **2018**, *16* (3), 1083–1088.
- (50) Grimme, S. Semiempirical GGA-type density functional constructed with a long-range dispersion correction. *J. Comput. Chem.* **2006**, 27 (15), 1787–1799.
- (51) Chai, J.-D.; Head-Gordon, M. Long-range corrected hybrid density functionals with damped atom—atom dispersion corrections. *Phys. Chem. Chem. Phys.* **2008**, *10* (44), 6615–6620.
- (52) Krishnan, R.; Binkley, J. S.; Seeger, R.; Pople, J. A. Self-consistent molecular orbital methods. XX. A basis set for correlated wave functions. *J. Chem. Phys.* **1980**, 72 (1), 650–654.
- (53) McLean, A. D.; Chandler, G. S. Contracted Gaussian basis sets for molecular calculations. I. Second row atoms, Z = 11–18. *J. Chem. Phys.* **1980**, 72 (10), 5639–5648.
- (54) Frisch, M. J.; et al. Gaussian 16; Gaussian, Inc.: Wallingford, CT, 2016.
- (55) Yanai, T.; Tew, D. P.; Handy, N. C. A new hybrid exchange—correlation functional using the Coulomb-attenuating method (CAM-B3LYP). *Chem. Phys. Lett.* **2004**, 393 (1), 51–57.
- (56) Barone, V.; Cossi, M. Quantum Calculation of Molecular Energies and Energy Gradients in Solution by a Conductor Solvent Model. *J. Phys. Chem. A* **1998**, *102* (11), 1995–2001.
- (57) Cossi, M.; Rega, N.; Scalmani, G.; Barone, V. Polarizable dielectric model of solvation with inclusion of charge penetration effects. *J. Chem. Phys.* **2001**, *114* (13), 5691–5701.
- (58) Dennington, R.; Keith, T. A.; Millam, J. M. Gaussview, 6.0.16; Semichem Inc.: Shawnee Mission, KS, 2016.
- (59) Sleszynski, N.; Zuman, P. Enol form of 2,3-butadione. *J. Org. Chem.* **1987**, 52 (12), 2622–2623.

- (60) Fay, L. B.; Huynh-Ba, T.; Blank, I. Study of the Fragmentation of 3(2H)-Furanones by Mass Spectrometry. *J. Agric. Food Chem.* 1997, 45 (10), 4057–4064.
- (61) Nozière, B.; Dziedzic, P.; Córdova, A. Inorganic ammonium salts and carbonate salts are efficient catalysts for aldol condensation in atmospheric aerosols. *Phys. Chem. Chem. Phys.* **2010**, *12* (15), 3864–3872.
- (62) Vas, C. A.; Porter, A.; McAdam, K. Acetoin is a precursor to diacetyl in e-cigarette liquids. Food Chem. Toxicol. 2019, 133, 110727.
- (63) Guerra, P. V.; Yaylayan, V. A. Double Schiff Base Adducts of 2,3-Butanedione with Glycine: Formation of Pyrazine Rings with the Participation of Amino Acid Carbon Atoms. *J. Agric. Food Chem.* **2012**, *60* (45), 11440–11445.
- (64) Swain, M. chemicalize.org. J. Chem. Inf. Model. 2012, 52 (2), 613-615.
- (65) SciFinder, version 2020; Chemical Abstracts Service: Columbus, OH, 2020, (Accessed June 2, 2020). Calculated using Advanced Chemistry Development (ACD/Labs), software, version 11.02; ACD/Labs 1994–2020.